Journal of Applied Physics

RESEARCH ARTICLE | JULY 22 2024

Influence of Xe^+ and Ga^+ milling species on the cathodoluminescence of wurtzite and zincblende GaN

Special Collection: Defects in Semiconductors 2024

K. Loeto ; S. M. Fairclough ; I. Griffiths; G. Kusch ; S. Ghosh ; M. J. Kappers ; N. Young; R. A. Oliver

J. Appl. Phys. 136, 045702 (2024)
https://doi.org/10.1063/5.0211529

05 August 2024 14:28:09

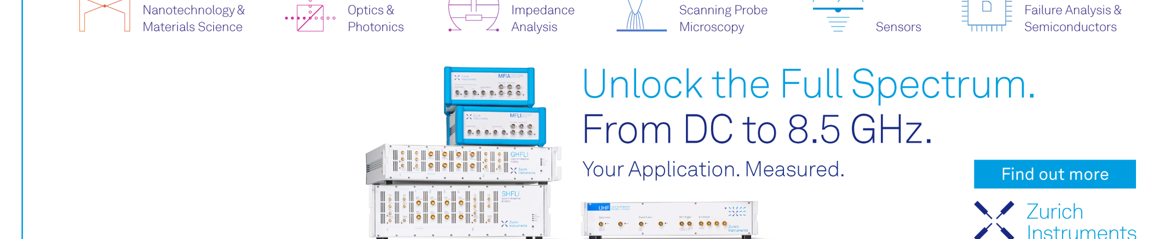

Journal of Applied Physics | ARTICLE | pubs.aip.org/aip/jap

Influence of Xe$^+$ and Ga$^+$ milling species on the cathodoluminescence of wurtzite and zincblende GaN

Cite as: J. Appl. Phys. **136**, 045702 (2024); doi: 10.1063/5.0211529
Submitted: 31 March 2024 · Accepted: 3 July 2024 ·
Published Online: 22 July 2024

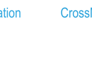
View Online Export Citation CrossMark

K. Loeto,[1,a)] S. M. Fairclough,[1] I. Griffiths,[2] G. Kusch,[1] S. Ghosh,[1] M. J. Kappers,[1] N. Young,[2] and R. A. Oliver[1]

AFFILIATIONS

[1]Department of Materials Science and Metallurgy, University of Cambridge, Cambridge, United Kingdom
[2]Department of Materials Science, University of Oxford, Oxford, United Kingdom

Note: This paper is part of the special topic, Defects in Semiconductors 2024.
[a)]**Author to whom correspondence should be addressed:** loeto@pdi-berlin.de

ABSTRACT

III-nitride materials, such as GaN and its alloys, are essential for modern microelectronics and optoelectronics due to their unique properties. Focused ion beam (FIB) techniques play a crucial role in their prototyping and characterization at the micro- and nanoscale. However, conventional FIB milling with Ga ions presents challenges, including surface amorphization and point defect introduction, prompting the exploration of alternative ion sources. Xenon-based inductively coupled plasma or plasma FIB has emerged as a promising alternative, offering reduced damage and better sample property preservation. Despite extensive research on FIB-induced damage in GaN, systematic comparisons between Ga and Xe ion milling on the luminescence characteristics of GaN remain limited. This study aims to fill this gap by evaluating and comparing the extent of FIB-induced damage caused by Ga and Xe ions in wurtzite and zincblende GaN through cathodoluminescence measurements. Our findings indicate that Xe ion milling yields higher integrated intensities compared to Ga ion milling, attributed to shallower implantation depths and reduced lattice disorder. We also observe a decrease in integrated intensity with increasing ion beam acceleration voltage for both wurtzite and zincblende GaN layers. This study provides valuable insights into optimizing FIB-based sample preparation techniques for III-nitride materials, with implications for enhancing device performance and reliability.

© 2024 Author(s). All article content, except where otherwise noted, is licensed under a Creative Commons Attribution-NonCommercial 4.0 International (CC BY-NC) license (https://creativecommons.org/licenses/by-nc/4.0/). https://doi.org/10.1063/5.0211529

05 August 2024 14:28:09

I. INTRODUCTION

The III-nitride materials, including GaN, AlN, InN, and their solid solutions, possess unique physical properties such as a wide bandgap, high carrier mobility, high breakdown fields, and excellent chemical stability, making them highly desirable for modern microelectronics and optoelectronics with applications ranging from high-power transistors to advanced solid-state lighting solutions.[1–5] To aid in the micro- and nanoscale prototyping and characterization of these materials to facilitate technological advancement, focused ion beam (FIB) can be applied. This is a high-resolution precision machining technique used to mill or sputter material away from the surface of a sample through the use of a high-energy and convergent ion beam.[6]

Conventional FIB milling has employed Ga liquid metal ion sources due to their extended operational lifetimes as well as the low volatility and melting temperature of Ga metal.[7,8] Nonetheless, the use of Ga ion sources presents challenges relating to lattice disorder that is initiated by collisions of high-momentum incident ions from the ion beam with the lattice atoms of the sample. The collisions transfer kinetic energy to the lattice atoms, displacing them from their lattice sites.[9,10] Referred to as a collision cascade, this process can generate simple defects such as vacancies and their associated interstitials. Alongside point defects, extended defects such as dislocation loops and stacking faults can also emerge, accompanied by an amorphous zone at the core of the collision cascade region.[9,10] The defects produced by collision cascade events

can further migrate through the material via dynamic annealing, leading to annihilation or the formation of defect clusters.[9] Moreover, Ga, being conductive and chemically active, can alter the electronic and chemical behavior of the semiconducting material but also makes chemical analysis of III-nitrides difficult as it becomes troublesome to distinguish from Ga intentionally present in the sample.[11,12]

These mechanisms result in a disturbed layer of material tens of nanometers thick, altering its structural, chemical, electronic, and optical properties compared to the unperturbed material.[13,14] Thus, there is demand for an alternative ion source to liquid metal Ga. Xenon-based inductively coupled plasma (ICP) or plasma FIB has emerged as a substitute for Ga due to its potential to limit the depth and degree of damage or lattice disorder on the sample. The atomic mass of Xe surpasses that of Ga, resulting in less surface amorphization and lower implantation depths for Xe plasma FIB compared to Ga.[9,15] Additionally, the greater mass of Xe enables ions to carry greater momentum, thereby increasing the milling rate and improving the technique's throughput.[15] Xe is also chemically inert, possesses lower conductivity, and does not significantly alter the chemistry and conductivity of the sample.[9]

Ion beam-induced damage in GaN has been investigated in the literature by techniques such as Rutherford backscattering spectrometry (RBS) and cross-sectional transmission electron microscopy (TEM) studies.[9,13] TEM has also been used to systematically study the damage induced in GaN by both Xe and Ga ions.[16] However, to the best of the authors' knowledge, there is little to no work in the literature that attempts to systematically examine and compare the effect of both Xe and Ga ion milling on the luminescence characteristics of GaN. This insight would be crucial for FIB-based sample preparation where it is important to maintain the optical emission characteristics such as in luminescence-based studies.

Point defects are believed to generate deep-level trap states within the bandgap of GaN, which function as Shockley–Read–Hall (SRH) recombination centers. Similarly, dislocations are also thought to introduce deep level states within the band-gap of GaN due to dangling bonds in the dislocation core.[17,18] It is also proposed that point defect atmospheres surrounding a dislocation could give rise to these deep-level states, subsequently functioning as SRH recombination centers akin to isolated point defects.[17] These deep-level states promote non-radiative recombination that leads to a reduction in the emission intensity of the GaN-near-band-edge (NBE) luminescence.[19] Thus, the objective of this work is to evaluate and compare the extent of FIB-induced damage caused by Ga and Xe ion species in GaN by analyzing the changes in optical emission intensity from cathodoluminescence (CL) measurements. Moreover, we aim to determine the optimal FIB conditions necessary to minimize such damage by controlling the ion beam acceleration voltage. Finally, the investigation will focus on both wurtzite and zincblende GaN layers as both crystalline phases have demonstrated utility in the design of III-nitride devices.[20]

II. METHODS

The wurtzite-GaN (wz-GaN) sample was grown on a 430 μm sapphire substrate in a metal organic vapor phase epitaxy (MOVPE) reactor employing trimethylgallium (TMGa) and NH_3 as Ga and N precursors, respectively, in a H_2 growth environment. After thermally annealing the substrate, a 30 nm wz-GaN nucleation layer was grown at 560 °C. The temperature was then ramped to 1060 °C to grow the full 1300 nm wz-GaN layer.

The zincblende-GaN (zb-GaN) sample was also grown in an MOVPE reactor. The substrate consisted of a 3 μm 3C-SiC layer on Si (001) with a misorientation of 4° toward [110]. TMGa, dicyclopentadienyl magnesium (Cp_2Mg), and NH_3 were used as Ga, Mg, and N precursors, respectively, while H_2 was used as the carrier gas. The two-step growth procedure comprised of thermal annealing of the substrate followed by a 40 nm low-temperature zb-GaN nucleation layer deposition at 600 °C. The temperature was then ramped to 880 °C to grow the zb-GaN epilayers, which were a 200 nm layer followed a 100 nm layer and finally a 500 nm Mg-doped zb-GaN layer.

FIB milling was carried out on both samples by employing a ThermoFisher G4-CXe plasma FIB and FEI Helios FIB microscope for Xe and Ga ion milling, respectively. The samples were mounted on a 45° pre-tilt holder to allow 7° bevels to be milled into the wz-GaN and zb-GaN samples. The bevels were produced on areas of approximately $20 \times 2\,\mu m^2$ for 20 min to ensure a uniform dose across the different FIB conditions. The ion beam current and acceleration voltage combinations chosen for both Ga and Xe FIB were 2, 0.2, and 0.02 nA with 30, 8, and 2 kV. Stopping and range of ions in matter (SRIM) ballistic calculations were also used to estimate the implantation depths of the Ga and Xe ions in both samples.[21] We define the implantation depth as the maximum depth of implanted Ga or Xe ions. Additionally, the integrated vacancy concentration produced by the ion-bombardment was also extracted from SRIM calculations.

CL measurements were recorded in an Attolight Allalin 4027 Chronos SEM-CL system at 300 K on the bevels from both samples. CL hyperspectral mapping was performed using an iHR320 spectrometer with a 150 lines per mm grating blazed at 500 nm. The CL measurements were recorded (at normal incidence) at a beam current of 5 nA and 5 kV acceleration voltage, which corresponds to 90% of the beam energy being deposited into a depth of ∼95 nm as determined by Monte Carlo simulations using *Monte Carlo Casino* software.[22] The CL hyperspectral datasets were analyzed using *HyperSpy*.[23]

III. CL ANALYSIS OF MANUALLY CLEAVED CROSS SECTIONS

Cleaved cross sections of the zb-GaN and wz-GaN samples were analyzed using CL hyperspectral mapping to understand the samples' luminescence properties prior to FIB bevelling. Figure 1(a) shows a secondary electron (SE) image of the zb-GaN cross section, while Fig. 1(b) presents the corresponding panchromatic CL map of the same area. The panchromatic CL map shows regions 1, 2, and 3, respectively, representing luminescence from the GaN:Mg (500 nm), GaN (100 nm), and GaN (200 nm) layers within the zb-GaN sample, as highlighted by the schematic in Fig. 1(c). The reduced emission intensity in region 1 compared to region 2 is attributed to Mg doping, which is known to increase the non-radiative point defect density in GaN, leading to a decrease in optical emission efficiency.[24] Similarly, the lower emission intensity

05 August 2024 14:28:09

© Author(s) 2024

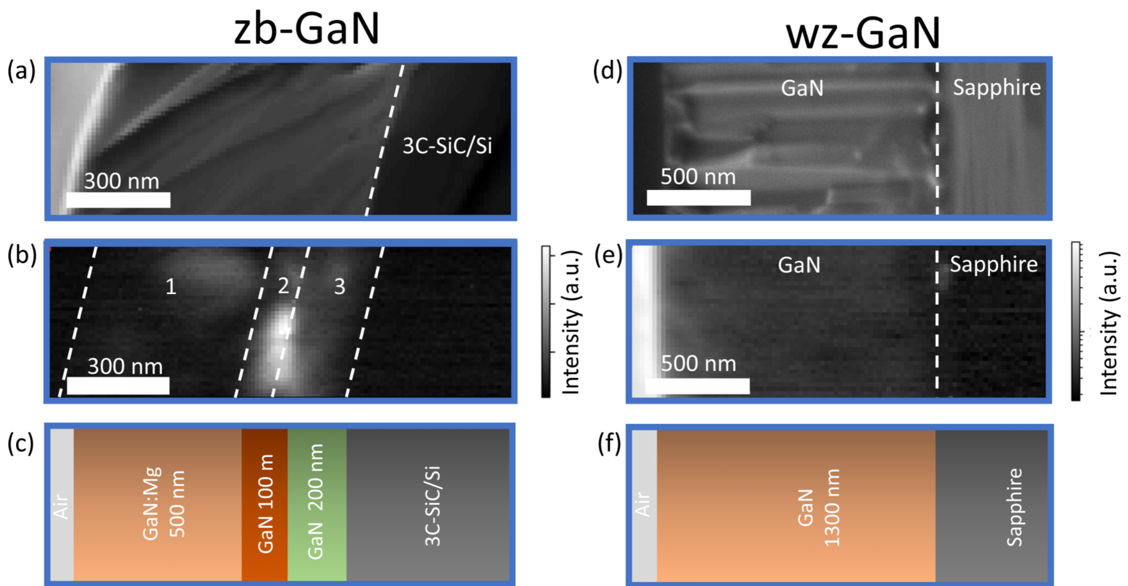

FIG. 1. (a) and (d) are SE images showing the cross sections of the zb-GaN and wz-GaN samples, respectively. The respective panchromatic CL maps for these samples are shown in (b) and (e). Regions 1, 2, and 3 are highlighted in (b), which correspond to the 3 GaN layers in the zb-GaN sample. (c) and (f) are the sample schematics for the zb-GaN and wz-GaN samples, respectively.

in region 3 can be attributed to an increase in non-radiative defects such as threading dislocations, which are expected to be more abundant closer to the substrate.

Figure 1(d) shows an SE image of the cleaved cross section taken from the wz-GaN sample, while Fig. 1(e) displays the corresponding panchromatic CL map of the same area. No significant spatial changes in luminescence intensity are observed in the panchromatic CL map. Instead, the 1300 nm wz-GaN layer in this sample exhibits a homogeneous spatial distribution of luminescence intensity. Figure 1(f) is a schematic of the wz-GaN sample.

To resolve the differences in optical emission among regions 1, 2, and 3 within the zb-GaN structure, mean CL spectra were extracted from these regions and are depicted in Fig. 2(a). Regions 1 and 2 exhibit similar spectral behavior, showing a typical narrow

05 August 2024 14:28:09

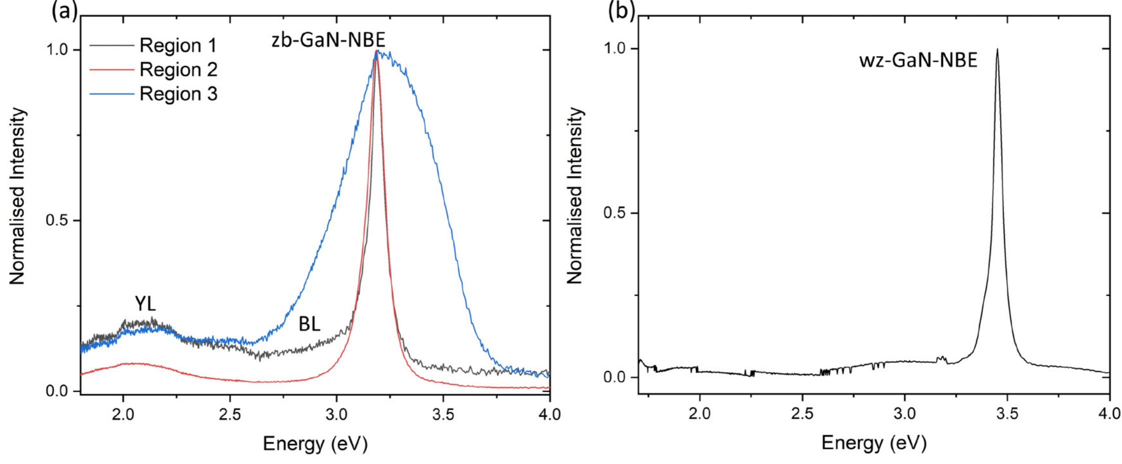

FIG. 2. (a) shows the mean spectra extracted from regions 1, 2, and 3 of the zb-GaN sample recorded from the field of view in Fig. 1(b). (b) is the mean spectrum extracted from the wz-GaN layer of the wz-GaN sample from the field of view in Fig. 1(e).

© Author(s) 2024

zb-GaN-NBE emission band at ∼3.2 eV and a yellow luminescence (YL) band at ∼2.1 eV. Additionally, region 1 also shows an additional blue luminescence (BL) band at ∼2.9 eV, which can be linked to Mg doping in zb-GaN.[25] Although region 3 also shows a YL band akin to regions 1 and 2, the zb-GaN-NBE band from this region is broader compared to those in regions 1 and 2. This broadening phenomenon has been previously observed in other zb-GaN layers near the 3C-SiC/Si interface and is attributed to an additional emission band at ∼3.3 eV corresponding to wz-GaN inclusions and an increased density of closely packed stacking faults near the substrate.[24–26] The density of stacking faults has been observed in literature to diminish with sample thickness away from the substrate due to reaction and annihilation.[24,27,28] Consequently, luminescence originating from stacking faults in zb-GaN most significantly impacts region 3. Although the presence of stacking faults can rationalize the shoulder observed near ∼3.3 eV, it is also possible that a high-density of native point defects in region 3 contributes to broadening observed that can rationalize the broadening observed in the lower energy side of this band.[29]

Figure 2(b) shows the mean spectrum obtained from the wz-GaN layer. The spectrum displays a typical wz-GaN-NBE luminescence band centered at ∼3.4 eV. No other luminescence bands can be observed from the wz-GaN mean spectrum.

To assess the zb-GaN-NBE CL intensity across the various FIB bevelling conditions to be studied and draw conclusions regarding the extent of ion-induced lattice disorder, region 1 can be utilized. This region, being the thickest (500 nm) layer in the zb-GaN sample, offers a larger sample space for averaging over compared to regions 2 (100 nm) and 3 (200 nm). Therefore, there is need to consistently differentiate between regions 1, 2, and 3 in the CL hyperspectral datasets under discussion to avoid inadvertently integrating over regions 2 and 3 during analysis. To achieve this, Gaussian curves were fitted to the spectrum in each pixel of the CL hyperspectral datasets corresponding to the field of view in Fig. 1(b). Subsequently, the peak intensity, center emission wavelength, and full width at half maximum (FWHM) of the zb-GaN-NBE were extracted and are presented in Fig. 3. The intensity trends observed in Fig. 3(a) align with those detailed above for the panchromatic CL map in Fig. 1(b), highlighting that they were dominated by NBE emission. Figures 3(b) and 3(c) reveal discernible differences in the center emission wavelength and FWHM behavior among regions 1, 2, and 3. However, the distinction is less pronounced between regions 1 and 2 due to their similar optical behavior, as previously highlighted by the spectra in Fig. 2(a). Conversely, the disparity is more significant for region 3 compared to regions 1 and 2 due to the influence of stacking faults and wz-GaN inclusions in this region.[24,26]

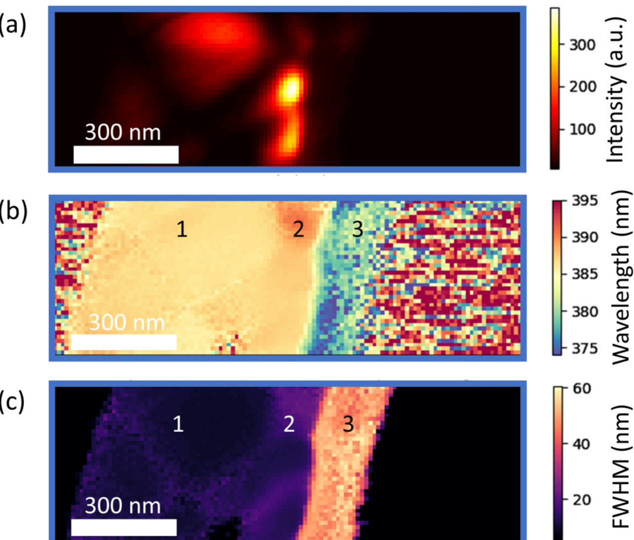

FIG. 3. (a), (b), and (c) are the respective peak intensity, centre emission wavelength, and FWHM maps extracted from the zb-GaN-NBE band of the zb-GaN sample by fitting Gaussian curves to the spectra in each pixel of the corresponding CL hyperspectral dataset.

IV. CL ANALYSIS OF BEVELLED CROSS SECTIONS

From SRIM calculations, the implantation depths were estimated at various FIB acceleration voltages taking into account the 7° incidence angle. The implantation depths are shown in Table I. Xe ion implantation depths are found to be lesser than those of Ga ions. This aligns with expectations due to the larger size of Xe ions.[9,15] The important insight obtained from these calculations is that the implantation depths of both species, across all conditions, remain significantly lower than the interaction volume of the electron beam, which is ∼95 nm. Consequently, direct electron beam excitation is expected to occur on both unperturbed and damaged material. Thus, the changes in wz- and zb-GaN-NBE intensity to be investigated can be linked to variations in both the degree of lattice disorder per unit volume introduced by FIB milling but also to changes in the volume of the damaged material with respect to the unperturbed material at a constant interaction volume.

Assessment of the lattice disorder induced by FIB milling will entail examining the changes in wz- and zb-GaN-NBE emission intensity resulting from variations in ion source and ion beam conditions. It is crucial to acknowledge that the intensity recorded from the samples depends on the electron beam alignment

05 August 2024 14:28:09

TABLE I. SRIM calculations[21] of the Ga and Xe ion implantation depths and integrated vacancy concentration at different FIB acceleration voltages and a 7° incidence angle. Here, we define the implantation depth as the maximum depth of implanted Ga or Xe ions.

Incident ion	Acceleration voltage (kV)	Implantation depth (nm)	Integrated vacancy concentration (cm^{-3})
Ga^+	30	44	34
	8	17	18
	2	6	8
Xe^+	30	30	35
	8	12	19
	2	5	9

© Author(s) 2024

conditions in the CL microscope, which may vary between experimental runs. Therefore, to mitigate this effect, the data under consideration were collected during the same session with approximately identical alignment and CL excitation conditions. This facilitates direct comparisons of the absolute CL intensities recorded.

CL hyperspectral mapping was performed on both the Xe and Ga ion produced bevels of the zb- and wz-GaN samples. Figure 4 presents data obtained from one such bevel recorded from the zb-GaN sample, which is considered representative of the other zb-GaN bevels. This particular bevel was generated using Xe ions at an ion beam current of 0.2 nA and an acceleration voltage of 2 kV. The SE image in Fig. 4(a) illustrates the bevel cross section. To identify region 1, Gaussian curves were fitted to the spectrum in each pixel of the CL hyperspectral dataset corresponding to the field of view in Fig. 4(a). From this analysis, the central emission wavelength and FWHM were extracted and illustrated in Figs. 4(c) and 4(d), respectively. Similar to observations made for the conventional cross section in Fig. 3, distinguishing between regions 1 and 2 proves challenging, while region 3 stands out distinctly due to its lower emission wavelength and larger FWHM. Given the inability to consistently differentiate region 1 from region 2 in this and other zb-GaN bevels, the subsequent analysis will be performed collectively from both regions disregarding region 3. Figure 4(b) is the panchromatic CL image corresponding to the field of view in (a). Here, the white rectangle denotes the region from which the mean spectrum was extracted for this bevel and similarly for the other zb-GaN bevels investigated. Note that this rectangle integrates over both regions 1 and 2 but excludes region 3. In addition, this region was maintained at a similar $\sim 2\,\mu m^2$ area for both zb- and wz-GaN bevels.

Figures 5(a) and 5(b) display the respective SE and panchromatic CL images captured for a Ga ion bevel on the wz-GaN sample. The CL data acquired from this bevel are considered representative of the other wz-GaN bevels. This particular bevel was created using Ga ions with an ion beam current of 2 nA and an acceleration voltage of 30 kV. Unlike the zb-GaN bevels, no fitting or region identification is necessary for the wz-GaN bevels as only a single wz-GaN layer with homogeneous emission properties is present in this sample, as evidenced by the panchromatic CL map in Fig. 5(b). The white rectangle in Fig. 5(b) denotes a typical region from which mean spectra were extracted from the wz-GaN bevels.

Figures 6(a) and 6(b) are representative mean spectra extracted from zb-GaN and wz-GaN bevels, respectively. Figure 6(a) shows those extracted from Xe bevels on the zb-GaN sample at an ion beam current of 0.2 nA and acceleration voltages of 2 and 30 kV. Figure 6(b) shows representative mean spectra extracted from Ga

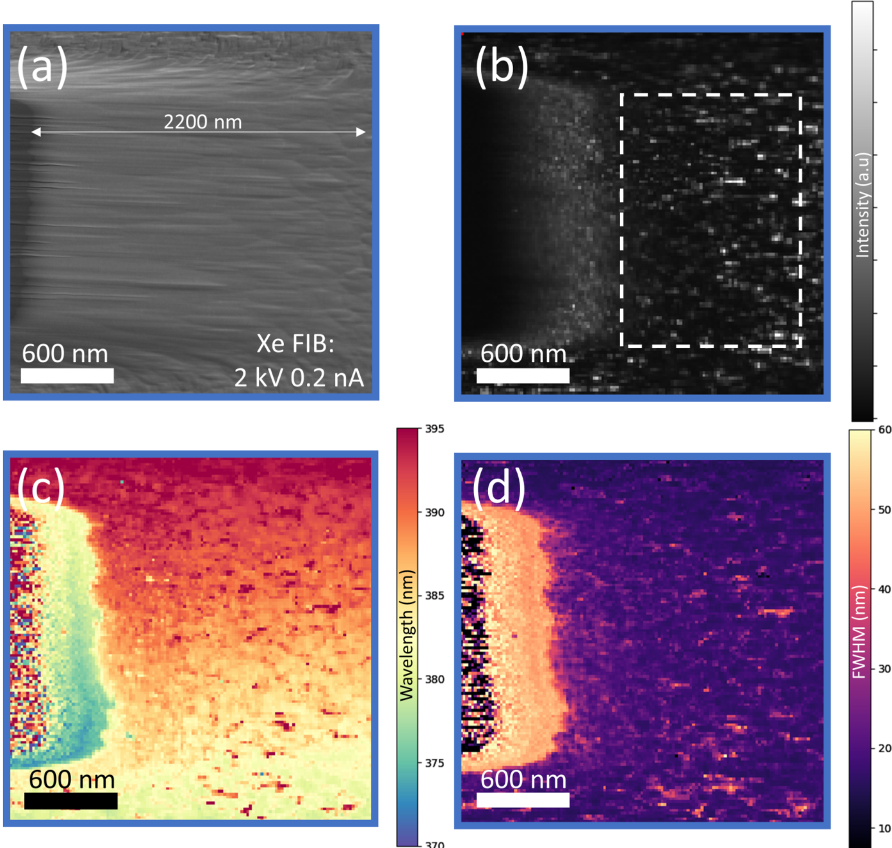

FIG. 4. (a) is an SE image showing a representative Xe FIB bevel on the zb-GaN sample. (b) is the corresponding panchromatic map of the same region in (a). The white rectangle shows the region within which a mean spectrum was extracted. (c) and (d) are the respective centre wavelength and FWHM maps extracted by fitting Gaussian curves to the CL hyperspectral dataset.

05 August 2024 14:28:09

© Author(s) 2024

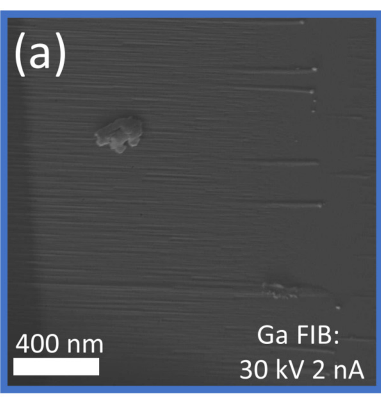

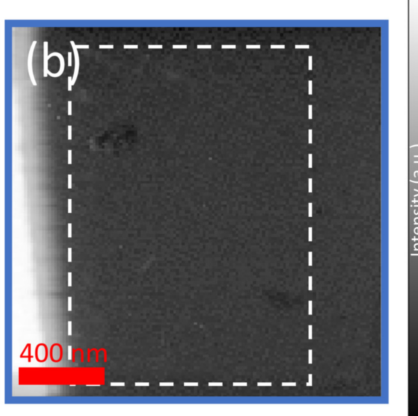

FIG. 5. (a) is an SE image showing a representative Ga FIB bevel on the wz-GaN sample. (b) is the corresponding panchromatic map of the same region in (a). The white rectangle shows the region within which a mean spectrum was extracted.

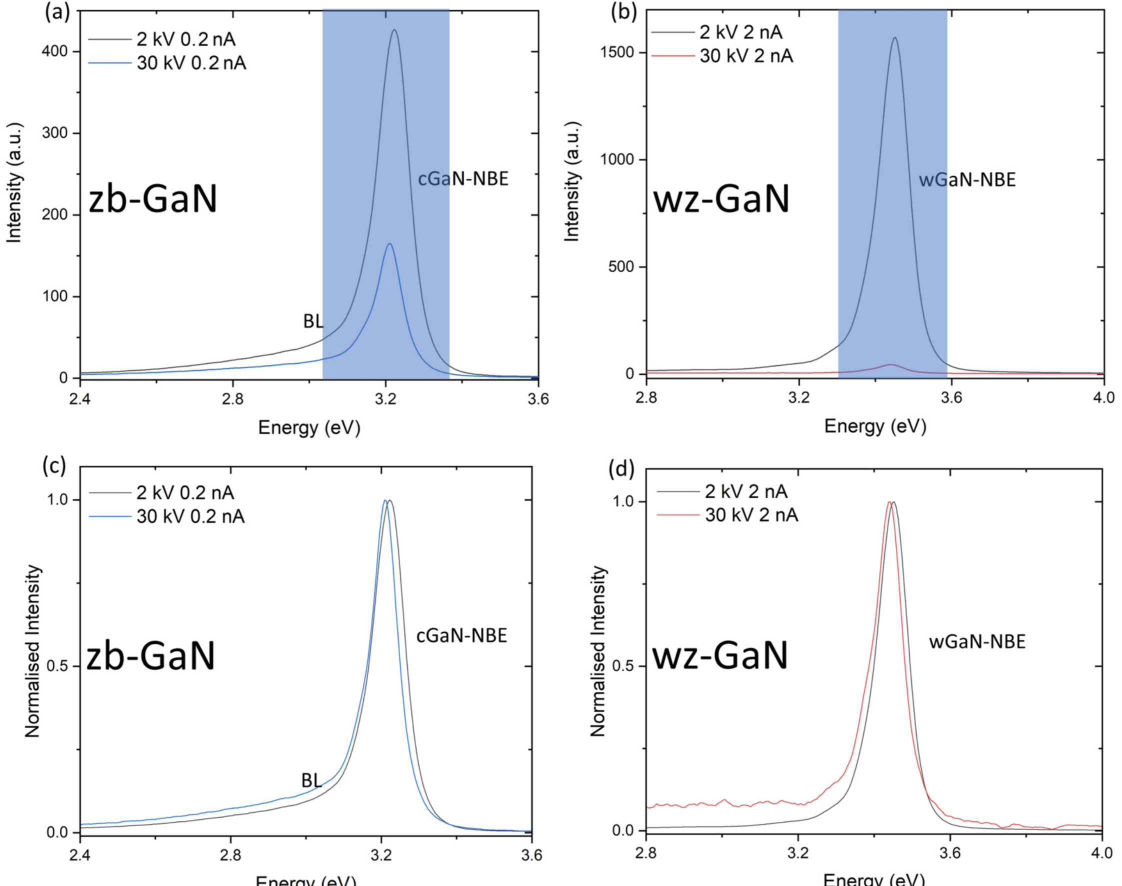

FIG. 6. (a) and (b) are representative mean spectra extracted from respective Xe and Ga bevels of the zb-GaN and wz-GaN samples. (c) and (d) are the respective normalized spectra to (a) and (b).

05 August 2024 14:28:09

© Author(s) 2024

ion bevels on the wz-GaN sample at an ion beam current of 2 nA and acceleration voltages of 2 and 30 kV. From spectra such as those shown in Figs. 6(a) and 6(b), the integrated intensity of the zb-GaN and wz-GaN NBE bands was extracted in spectral regions such as that shown by the highlighted range in both figures and for the other bevels investigated. Note that there were no significant changes in the profile of these spectra for all bevels investigated such that similar integration energy ranges could be applied at all FIB conditions. This can be highlighted by considering Figs. 6(c) and 6(d), which are the representative normalized mean spectra from (a) and (b). The CL spectra for all FIB conditions are included in the supplementary material for completeness.

Figures 7(a) and 7(b) are the integrated GaN-NBE intensities calculated for all Xe and Ga ion bevels on both zb-GaN and wz-GaN. The comparison encompasses bevels produced using ion beam currents of 2, 0.2, and 0.02 nA as well as acceleration voltages of 2, 8, and 30 kV. It is highlighted here that some FIB current data points are missing in Fig. 7 due to some difficulties encountered during the milling process. Across all FIB conditions depicted in both figures, it is consistently observed that the integrated GaN-NBE intensities calculated from Xe ion bevels (triangles) surpass those of Ga ion bevels (squares).

The GaN-NBE CL intensity is dependent upon the degree of lattice disorder and is anticipated to diminish with escalating FIB-induced damage.[9,10,30] This phenomenon arises because lattice disorder introduces non-radiative defects like point defects and dislocations that enhance the degree non-radiative recombination compared to radiative recombination.[19,31,32] Compared to Ga ions, Xe ions are believed to contribute to a reduced lattice disorder and damage depths due to their larger atomic mass or higher momentum at the same acceleration voltage.[9,15] The lower damage depths were previously demonstrated through ballistic calculations in Table I. Therefore, the higher integrated intensities observed for Xe ions in Figs. 7(a) and 7(b) can be attributed to decreased lattice disorder and damage depths compared to Ga ions.

With that said, it is crucial to acknowledge that the majority of the material being directly stimulated by the CL electron beam is unperturbed. This is because at the chosen electron beam acceleration voltage of 5 kV, the interaction volume was ~95 nm, which is more than twice the largest estimated ion implantation depths in Table I. Consequently, spatial variations in the distribution of non-radiative recombination centers within the unperturbed material can also contribute to the observed intensity variations. This effect is particularly notable for the zb-GaN sample. As illustrated in the conventional cross sections in Figs. 1(b) and 3(a), there exists a more pronounced spatial variability in luminescence intensity within regions 1 and 2 for the zb-GaN sample compared to the more homogeneous distribution observed in the wz-GaN sample depicted in Fig. 1(d). However, it is worth noting that the bevel mean spectra in the zb-GaN sample were extracted from larger areas of approximately $\sim 2\,\mu m^2$ in contrast to the $\sim 0.35\,\mu m^2$ areas analyzed in the conventional cross sections. Consequently, the intensity variations observed in Figs. 1(b) and 3(a) may be insignificant for larger areas. Indeed, this tendency is evident from the panchromatic CL image in Fig. 4(b), which exhibits a more homogeneous spatial variation of intensity within the region marked by the white rectangle.

It is noted here that an acceleration voltage of 5 kV was chosen to optimize the luminescence intensity received from both samples at all FIB bevels. The CL data recorded at lower acceleration voltages such as 3 kV showed a lower signal-to-noise ratio and could, thus, not be used. The lower CL signal received at 3 kV can be related to a reduction in the carrier generation rate that scales with the acceleration voltage.[33] However, this can also be related to a reduction in the volume of unperturbed material that is directly excited by the electron beam. From Monte Carlo simulations, at 3 kV, the interaction volume would now be ~45 nm instead of ~95 nm calculated at 5 kV. This means that the non-radiative layer of damaged material, which is thought to be near the surface, now contributes more with regard to decreasing the recorded CL signal.[13]

05 August 2024 14:28:09

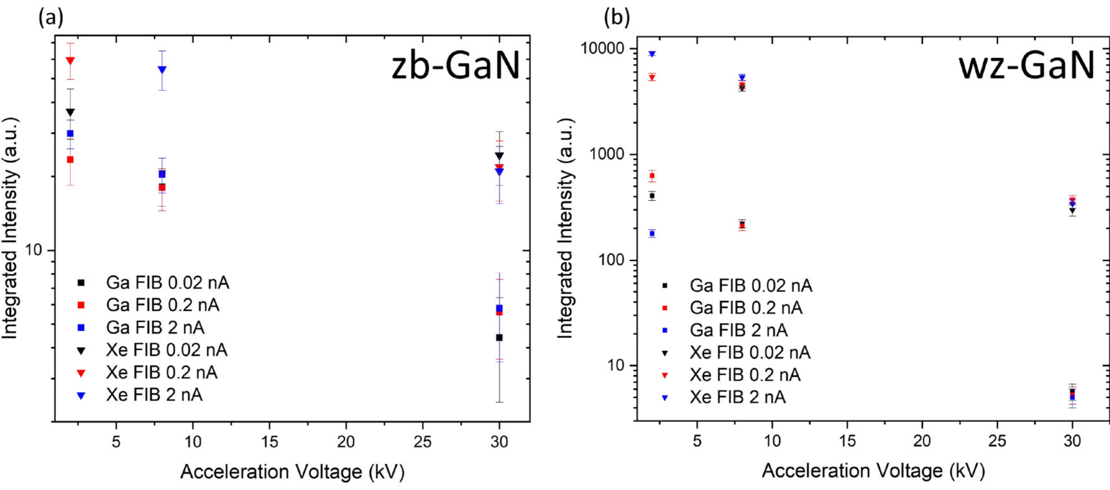

FIG. 7. (a) and (b) compare the integrated intensities extracted from the Xe and Ga ion bevels for the zb-GaN and wz-GaN samples, respectively.

© Author(s) 2024

A smaller acceleration voltage such as 3 kV with an interaction volume of ∼45 nm could aid in providing a means to quantify the degree of lattice disorder produced by the milling process when compared to the unperturbed material. This is because more of the perturbed material will be probed with respect to the interaction volume especially at 30 kV FIB acceleration voltage, thus providing a more direct comparison than at 5 kV. However, the reduction in recorded CL intensity at 3 kV makes this difficult to achieve. In addition, for this work, the unperturbed integrated intensity obtained from the manually cleaved cross sections in Fig. 1 could also not be directly compared to those in Fig. 7. This is because it was difficult to produce pristine cleaved surfaces and only heavily defected cleaved cross section were produced. For instance, integrated intensities of ∼15 and ∼5 were recorded for the cleaved cross sections of zb-GaN and wz-GaN, respectively. These are much lower than all values recorded at 2 kV using both ion species in Fig. 7, for instance. More controlled methods such as laser scribing could provide a means to produce more pristine cross sections allowing such comparisons to be made. In any case, the average relative improvement in integrated CL intensity (ignoring differences in FIB current) obtained from using Xe ions compared to Ga ions were calculated and are shown in Table II for both polytypes at each FIB acceleration voltage.

Also noted from Fig. 7 is the trend of decreasing integrated GaN-NBE intensity with an increase in the ion beam acceleration voltage for both zb-GaN and wz-GaN samples. This phenomenon can be linked to the dependence of the depth and degree of lattice disorder on the kinetic energy of the incident ions.[13] Higher kinetic energies of incident ions result in deeper implantation depths owing to the increased momentum carried by the ions as seen by the trend in implantation depth with acceleration voltage from Table I. Furthermore, a greater amount of kinetic energy can be transferred to the lattice atoms, leading to an increased degree of atomic displacements and consequent lattice disorder as seen by the trend in integrated vacancy concentration from Table I.[9,10] Hence, it can be deduced that augmenting the acceleration voltage or incident ion kinetic energy influences the density of non-radiative defects in both zb-GaN and wz-GaN samples. It is noted that the extracted integrated vacancy concentrations from both Ga and Xe ion bombardment shown in Table I are similar at each FIB acceleration voltage. However, Fig. 7 shows a greater integrated CL intensity reduction for the Ga compared to the Xe ions. This is because SRIM is only a ballistic approach and does not consider other relevant phenomena such as dynamic annealing, the formation of point defect complexes and dislocation loops, amorphization, and the differences in chemical activity between Ga and Xe ions[9–12]

TABLE II. The average relative improvement in integrated CL intensity obtained by utilizing Xe ions compared to Ga ions at each FIB acceleration voltage for zb-GaN and wz-GaN.

Polytype	Acceleration voltage (kV)	Relative intensity improvement
zb-GaN	30	∼4
	8	∼3
	2	∼9
wz-GaN	30	∼63
	8	∼22
	2	∼18

V. CONCLUSIONS

In conclusion, our study utilized CL hyperspectral mapping to evaluate the lattice disorder induced by FIB milling on both wz-GaN and zb-GaN samples, with a specific focus on comparing the effects of Xe and Ga primary ions. Through the analysis of mean spectra extracted from FIB milled bevels and comparison of integrated intensities, it was evident that Xe ion milling resulted in higher integrated intensities compared to Ga ion milling across all FIB conditions for both types of GaN samples. This feature can be attributed to the larger atomic mass and reduced chemical activity of Xe ions, which led to shallower implantation depths and reduced degree of lattice disorder compared to Ga ions. This finding underscores Xe as the preferred primary ion for FIB-based sample preparation, particularly when preserving the structural and optical properties of the sample surface is essential. While assessing the impact of FIB milling on CL measurements, it was crucial to consider that the majority of the probed material remained unperturbed. This understanding was based on theoretical implantation depths and Monte Carlo simulations. Although inhomogeneities in non-radiative recombination centers could introduce errors in integrated intensity recordings, our analysis indicated minimal effects due to averaging over relatively large areas. To optimize our technique further, expanding the milled area to mitigate potential errors may be beneficial, albeit at the expense of increased milling times. Additionally, our observations revealed a decrease in integrated intensity with increasing ion beam acceleration voltage for both wz-GaN and zb-GaN samples, regardless of the primary ion species. This trend was linked to deeper implantation depths and heightened lattice disorder induced by the escalating kinetic energy of primary ions. In summary, our study provides valuable insights into optimizing FIB-based sample preparation techniques for CL analysis, shedding light on the influence of primary ion species and ion beam acceleration voltage on lattice disorder in GaN samples.

05 August 2024 14:28:09

SUPPLEMENTARY MATERIAL

See the supplementary material for cathodoluminescence spectra extracted from all Ga and Xe FIB bevels on both zb-GaN and wz-GaN.

ACKNOWLEDGMENTS

This research was supported by the EPSRC under Grant No. EP/R025193/1 and Cambridge NanoDTC No. EP/S022953/1. Kagiso Loeto would like to acknowledge the Botswana government for his Ph.D funding. Dr. Christian Monachon of Attolight is thanked for his ongoing support of the CL system.

AUTHOR DECLARATIONS

Conflict of Interest

The authors have no conflicts to disclose.

© Author(s) 2024

Author Contributions

K. Loeto: Conceptualization (lead); Formal analysis (lead); Investigation (lead); Methodology (lead); Writing – original draft (lead); Writing – review & editing (lead). **S. M. Fairclough:** Conceptualization (equal); Formal analysis (supporting); Investigation (equal); Methodology (equal); Writing – review & editing (supporting). **I. Griffiths:** Investigation (equal); Methodology (equal); Writing – review & editing (supporting). **G. Kusch:** Formal analysis (equal); Supervision (equal); Writing – review & editing (equal). **S. Ghosh:** Investigation (equal); Writing – review & editing (equal). **M. J. Kappers:** Investigation (equal); Writing – review & editing (equal). **N. Young:** Conceptualization (equal); Writing – review & editing (equal). **R. A. Oliver:** Conceptualization (equal); Formal analysis (equal); Funding acquisition (equal); Supervision (equal); Writing – review & editing (equal).

DATA AVAILABILITY

The data that support the findings of this study are available within the article.

REFERENCES

[1]R. Pengelly, S. Wood, J. Milligan, S. Sheppard, and W. Pribble, "A review of GaN on SiC high electron-mobility power transistors and MMICs," IEEE Trans. Microwave Theory Tech. **60**, 1764–1783 (2012).
[2]M. Ishida, T. Ueda, T. Tanaka, and D. Ueda, "GaN on Si technologies for power switching devices," IEEE Trans. Electron Devices **60**, 3053–3059 (2013).
[3]M. Kuzuhara, J. T. Asubar, and H. Tokuda, "AlGaN/GaN high-electron-mobility transistor technology for high-voltage and low-on-resistance operation," Jpn. J. Appl. Phys. **55**, 070101 (2016).
[4]T. Mukai, M. Yamada, and S. Nakamura, "Characteristics of InGaN-based UV/Blue/Green/Amber/Red light-emitting diodes," Jpn. J. Appl. Phys. **38**, 3976–3981 (1999).
[5]S. C. Jain, M. Willander, J. Narayan, and R. V. Overstraeten, "III–nitrides: Growth, characterization, and properties," J. Appl. Phys. **87**, 965–1006 (2000).
[6]D. C. Cox, *Introduction to Focused Ion Beam Nanometrology* (Morgan & Claypool Publishers, 2015), 2053–2571.
[7]B. Knuffman, A. V. Steele, and J. J. McClelland, "Cold atomic beam ion source for focused ion beam applications," J. Appl. Phys. **114**, 044303 (2013).
[8]*Introduction to Focused ion Beams: Instrumentation, Theory, Techniques and Practice*, edited by L. A. Giannuzzi and F. A. Stevie (Springer, Boston, MA, 2005).
[9]S. Kucheyev, J. Williams, and S. Pearton, "Ion implantation into GaN," Mater. Sci. Eng. R **33**, 51–108 (2001).
[10]C. Ronning, E. Carlson, and R. Davis, "Ion implantation into gallium nitride," Phys. Rep. **351**, 349–385 (2001).
[11]S. Rubanov and P. Munroe, "Damage in III–V compounds during focused ion beam milling," Microsc. Microanal. **11**, 446–455 (2005).
[12]A. Ernst, M. Wei, and M. Aindow, "A comparison of Ga FIB and Xe-plasma FIB of complex Al alloys," Microsc. Microanal. **23**, 288–289 (2017).
[13]T. Sato, K. Nakano, H. Matsumoto, S. Torikawa, I. Nakatani, M. Kiyohara, and T. Isshiki, "High quality lamella preparation of gallium nitride compound semiconductor using triple Beam™ system," J. Phys.: Conf. Ser. **902**, 012019 (2017).
[14]D. D. E. Winter, M. Lebbink, D. W. D. E. Vries, J. Post, and M. Drury, "FIB-SEM cathodoluminescence tomography: Practical and theoretical considerations," J. Microsc. **243**, 315–326 (2011).
[15]R. Kelley, K. Song, B. Van Leer, D. Wall, and L. Kwakman, "Xe^+ FIB milling and measurement of amorphous silicon damage," Microsc. Microanal. **19**, 862–863 (2013).
[16]S. Jiang and V. Ortalan, "A comparative study of gallium-, xenon-, and helium-focused ion beams for the milling of GaN," Nanomaterials **13**, 2898 (2023).
[17]E. B. Yakimov, P. S. Vergeles, A. Y. Polyakov, I. V. Shchemerov, A. Chernyh, A. Vasilev, A. Kochkova, I.-H. Lee, and S. Pearton, "Dislocations introduced in n-GaN at room temperature cause conductivity inversion," J. Alloys Compd. **877**, 160281 (2021).
[18]J. Lähnemann, V. M. Kaganer, K. K. Sabelfeld, A. E. Kireeva, U. Jahn, C. Chèze, R. Calarco, and O. Brandt, "Carrier diffusion in GaN: A cathodoluminescence study. III. Nature of nonradiative recombination at threading dislocations," Phys. Rev. Appl. **17**, 024019 (2022).
[19]I.-H. Lee, A. Y. Polyakov, N. B. Smirnov, I. V. Shchemerov, P. B. Lagov, R. A. Zinov'ev, E. B. Yakimov, K. D. Shcherbachev, and S. J. Pearton, "Point defects controlling non-radiative recombination in GaN blue light emitting diodes: Insights from radiation damage experiments," J. Appl. Phys. **122**, 115704 (2017).
[20]B. Ding, "Improving radiative recombination efficiency of green light-emitting diodes," Mater. Sci. Technol. **34**, 1615–1630 (2018).
[21]J. F. Ziegler, M. Ziegler, and J. Biersack, "SRIM –the stopping and range of ions in matter (2010)," in *19th International Conference on Ion Beam Analysis* (Nuclear Instruments and Methods in Physics Research Section B: Beam Interactions with Materials and Atoms, 2010), Vol. 268, pp. 1818–1823.
[22]D. Drouin, A. R. Couture, D. Joly, X. Tastet, V. Aimez, and R. Gauvin, "CASINO V2.42—A fast and easy-to-use modeling tool for scanning electron microscopy and microanalysis users," Scanning **29**, 92–101 (2007).
[23]F. D. L. Peña, V. T. Fauske, P. Burdet, E. Prestat, P. Jokubauskas, M. Nord, T. Ostasevicius, K. E. MacArthur, M. Sarahan, D. N. Johnstone, J. Taillon, A. Eljarrat, V. Migunov, J. Caron, T. Furnival, S. Mazzucco, T. Aarholt, M. Walls, T. Slater, F. Winkler, B. Martineau, G. Donval, R. McLeod, E. R. Hoglund, I. Alxneit, I. Hjorth, T. Henninen, L. F. Zagonel, A. Garmannslund, and A. Skorikov, "Hyperspy/hyperspy: HyperSpy v1.5.2" (2018).
[24]B. Ding, M. Frentrup, S. M. Fairclough, G. Kusch, M. J. Kappers, D. J. Wallis, and R. A. Oliver, "Multimicroscopy of cross-section zincblende GaN LED heterostructure," J. Appl. Phys. **130**, 115705 (2021).
[25]Y. Hu, C. A. Hernández-Gutiérrez, H. Solís-Cisneros, G. Santana, Y. Kudriatsev, J. Camas-Anzueto, and M. López-López, "Blue luminescence origin and Mg acceptor saturation in highly doped zinc-blende GaN with Mg," J. Alloys Compd. **897**, 163133 (2022).
[26]S. A. Church, S. Hammersley, P. W. Mitchell, M. J. Kappers, L. Y. Lee, F. Massabuau, S. L. Sahonta, M. Frentrup, L. J. Shaw, D. J. Wallis, C. J. Humphreys, R. A. Oliver, D. J. Binks, and P. Dawson, "Effect of stacking faults on the photoluminescence spectrum of zincblende GaN," J. Appl. Phys. **123**, 185705 (2018).
[27]P. Vacek, M. Frentrup, L. Y. Lee, F. C.-P. Massabuau, M. J. Kappers, D. J. Wallis, R. Gröger, and R. A. Oliver, "Defect structures in (001) zincblende GaN/3C-SiC nucleation layers," J. Appl. Phys. **129**, 155306 (2021).
[28]L. Y. Lee, M. Frentrup, P. Vacek, M. J. Kappers, D. J. Wallis, and R. A. Oliver, "Investigation of stacking faults in MOVPE-grown zincblende GaN by XRD and TEM," J. Appl. Phys. **125**, 105303 (2019).
[29]E. Baron, R. Goldhahn, M. Deppe, D. J. As, and M. Feneberg, "Photoluminescence line-shape analysis of highly n-type doped zincblende GaN," Phys. Status Solidi B **257**, 1900522 (2020).
[30]S. O. Kucheyev, M. Toth, M. R. Phillips, J. S. Williams, C. Jagadish, and G. Li, "Cathodoluminescence depth profiling of ion-implanted GaN," Appl. Phys. Lett. **78**, 34–36 (2001).
[31]T. Miyajima, T. Hino, S. Tomiya, K. Yanashima, H. Nakajima, Y. Nanishi, A. Satake, Y. Masumoto, K. Akimoto, T. Kobayashi, and M. Ikeda, "Threading dislocations and optical properties of GaN and GaInN," Phys. Status Solidi B **228**, 395–402 (2001).
[32]D. Cherns, S. J. Henley, and F. A. Ponce, "Edge and screw dislocations as non-radiative centers in InGaN/GaN quantum well luminescence," Appl. Phys. Lett. **78**, 2691–2693 (2001).
[33]C. J. Wu and D. B. Wittry, "Investigation of minority-carrier diffusion lengths by electron bombardment of Schottky barriers," J. Appl. Phys. **49**, 2827–2836 (2008).

05 August 2024 14:28:09

© Author(s) 2024